

Half-metallicity in NiMnSb: a Variational Cluster Approach with ab-initio parameters

H. Allmaier,^{1,*} L. Chioncel,^{1,2} E. Arrigoni,¹ M.I. Katsnelson,³ and A.I. Lichtenstein⁴

¹*Institute of Theoretical Physics, Graz University of Technology, A-8010 Graz, Austria*

²*Faculty of Science, University of Oradea, RO-47800, Romania*

³*Institute for Molecules and Materials, Radboud University of Nijmegen, NL-6525 ED Nijmegen, Netherlands*

⁴*Institute of Theoretical Physics, University of Hamburg, 20355 Hamburg, Germany*

Electron correlation effects in the half-metallic ferromagnet NiMnSb are investigated within a combined density functional and many-body approach. Starting from a realistic multi-orbital Hubbard-model including *Mn* and *Ni-d* orbitals, the many-body problem is addressed via the Variational Cluster Approach. The density of states obtained in the calculation shows a strong spectral weight transfer towards the Fermi level in the occupied conducting majority spin channel with respect to the uncorrelated case, as well as states with vanishing quasiparticle weight in the minority spin gap. Although the two features produce competing effects, the overall outcome is a strong reduction of the spin polarisation at the Fermi level with respect to the uncorrelated case. This result emphasizes the importance of correlation in this material.

I. INTRODUCTION

More than twenty years ago *de Groot et al.*¹ carried out electronic structure calculations for the half-Heusler compound NiMnSb which showed peculiar magnetic features leading to the discovery of a new class of materials, the so-called half-metallic ferromagnets. Such materials differ from conventional ferromagnets in that they display a gap in one of the spin channels only. The concept of half metallicity boosted the research in spintronics - an emergent technology which makes use of spin and charge of electrons at the same time. Spintronic applications such as spin-valves, polarized electron injectors/detectors or devices using tunneling and giant magneto-resistance effects promise to revolutionize microelectronics once highly polarized electrons can be injected efficiently at room temperatures^{2,3}.

Unfortunately, the theoretically predicted ideal full spin polarization of half-metals has not yet been found experimentally. As a matter of facts, experiments show that full polarization is lost at temperatures of the order of room temperature, and even at lower temperatures different factors such as structural inhomogeneities, as well as surfaces and interface properties may suppress it^{4,5}.

Despite the fact that high quality NiMnSb films have been successfully grown, they were not found to reproduce the half-metallic character of the bulk suggested by spin-polarized positron-annihilation^{6,7}. Values of spin polarization were reported between 40% in spin-resolved photoemission measurements⁸ up to $58 \pm 2.3\%$ by superconducting point contact measurements at low temperatures² (see also Refs. 9,10). The discrepancy between theoretical calculations¹ and the above mentioned experimental facts were attributed to surface and interface effects. Consequently, different surface and interfaces of NiMnSb were theoretically investigated by *de Wijs* and *de Groot*⁴, which demonstrated that half-metallicity can be preserved at the surface and/or interface by suitable reconstruction⁴. The theoretical situation is complicated

by the fact that the spin polarisation (or, more precisely the tunneling magnetoresistance) displays a substantial uniaxial anisotropy in this material.¹¹

Recently, finite-temperature correlation effects were addressed in several half-metals^{5,12,13,14,15,16}. For NiMnSb, a Local Density Approximation plus Dynamical Mean Field Theory calculation (LDA+DMFT)¹² showed the appearance of so-called non-quasiparticle (NQP) states. These states originate from spin-polaron processes^{17,18}, whereby the spin-down low-energy electron excitations, which are forbidden for half-metallic ferromagnets in the one-particle picture, turn out to be possible as superpositions of spin-up electron excitations and virtual magnons^{5,17,18}. Here, we extend this study by adopting the Variational Cluster Approach (VCA), which includes correlations beyond the locality captured by DMFT. In addition, the VCA is based on exact diagonalisation, which is more appropriate than the diagrammatic method (FLEX) adopted in Ref. 12 to solve the impurity problem. In a previous paper,¹⁹ we used the VCA to investigate the spin polarization in NiMnSb taking into account only the *Mn-d* orbital basis set. Our calculations showed that the *Mn-d*-only basis set is not sufficient to appropriately describe the low energy spectrum of NiMnSb around the Fermi level. For this reason, in the present work we adopt a multi-orbital Hubbard-type Hamiltonian which includes all 10 *Mn* and *Ni-d* orbitals. Our present calculation confirms that the inclusion of the latter is essential for a proper description of ferromagnetic properties and of the minority spin gap in NiMnSb.

Our results support the existence of states within the minority spin gap in agreement with previous LDA+DMFT calculations^{5,12}. In addition, they indicate that these so-called nonquasiparticle states indeed have a vanishing quasiparticle weight at the Fermi energy. At the same time, our results predict a correlation-induced spectral weight transfer for the majority spin states. The combination of these two effects yields a

polarization whose energy dependence is in qualitative agreement with experiments. These calculations lead to the conclusion that even in the presence of medium-size interactions, electron correlations significantly affect the spin polarisation in half-metals.

This paper is organized as follows: in section II we present the methods used to investigate the electronic structure of NiMnSb. In particular, in Sec. II A we describe the *ab-initio* construction of the many-body model Hamiltonian. Specifically, the uncorrelated part of the Hamiltonian for excitations in the vicinity of the Fermi level is obtained from the so-called downfolding technique^{20,21} within the Nth-order muffin tin orbital (NMTO) method. In Sec. II B, we give a short summary of the VCA approach. We present and discuss our results in Sec. III. In particular, in Sec. III A, we evaluate the density of states within VCA and discuss the results in the framework of previous calculations. In Sec. III B we discuss *k*-dependent spectral properties, namely the spectral function and the self-energy. Finally, spin polarization and its comparison with experiments is discussed in Sec. III C, and the summary of the results is presented in Sec. IV.

II. ELECTRONIC STRUCTURE CALCULATIONS FOR NIMNSB

The intermetallic compound *NiMnSb* crystallizes in the cubic structure of *MgAgAs* type ($C1_b$) with the *fcc* Bravais lattice (space group $F\bar{4}3m = T_d^2$). This structure can be described as three interpenetrating *fcc* lattices of *Ni*, *Mn* and *Sb* with the lattice parameter $a = 11.20a_0$ ($a_0 = \text{Bohr radius}$), respectively. The *Ni* and *Sb* sublattices are shifted relative to the *Mn* sublattice by a quarter of the [111] diagonal in opposite directions, see also Fig. 1. The important aspects^{1,5,22,23,24,25} which determine the behavior of electrons near the Fermi level, as well as the half-metallic properties are the interplay between the crystal structure, the valence electron count, the covalent bonding, and the large exchange splitting of *Mn-d* electrons. For the minority spin gap opening, not only the *Mn-d-Sb-p* interactions, but also *Mn-d-Ni-d* interactions have to be taken into account. In addition, the loss of inversion symmetry produced by the $C1_b$ structure (the symmetry lowering from O_h in the $L2_1$ structure to T_d in the $C1_b$ structure) are important for these effects. The existence of *sp*-valent *Sb* is crucial to provide stability to this compound.

The crystal structure is shown in Fig. 1. The positions occupied by atoms are represented by spheres. For illustrative purposes, in Fig. 1 the radii of the spheres were chosen arbitrarily. The actual muffin-tin radii used in the calculations are $R_{MT}^{Ni} = 2.584$; $R_{MT}^{Mn} = 2.840$; $R_{MT}^{Sb} = 2.981$ and $R_{MT}^E = 2.583$ (atomic units) for the vacant position situated in $(1/4, 1/4, 1/4)$. The LMTO-ASA basis used for the self-consistent calculations contains the *spd*-partial waves for *Mn* and *Ni*, the *sp(df)*-partial waves

for *Sb* and *s(pd)*-partial waves for the empty sphere *E*. (*l*) means that the *l*-partial waves are downfolded within the selfconsistent calculations.

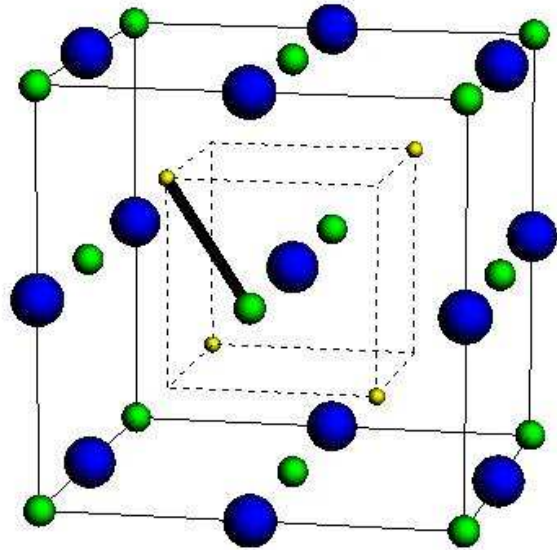


FIG. 1: (Color online) The conventional unit cell for the semi-Heusler NiMnSb compound: *Sb* (large, blue spheres) and *Mn* (medium, green spheres) sit on the same faces of the large cube (shown with thin, solid lines), *Ni* (small, yellow spheres) forms a separate (small) cube drawn using dashed lines. In addition, the atoms belonging to the reference system of the VCA calculation are connected by a thick solid line. *Sb* orbitals are downfolded and, therefore, not included directly in the model calculation.

A. Ab-initio construction of the model Hamiltonian

In order to construct the effective low-energy Hamiltonian to use in our VCA calculation, we employed the Nth order muffin-tin-orbitals scheme within the LMTO-ASA basis set²⁶. The NMTO method^{20,21} can be used to generate truly minimal basis sets with a massive downfolding technique. Downfolding produces minimal bands which follow exactly the bands obtained with the full basis set. The minimal set of symmetrically orthonormalized NMTOs is a set of Wannier functions. In the construction of the NMTO basis set the active channels are forced to be localized onto the eigenchannel $\mathbf{R}lm$, making the NMTO basis set strongly localized.

Fourier-transformation of the orthonormalized NMTO Hamiltonian, $H^{LDA}(\mathbf{k})$, yields on-site energies and hopping integrals,

$$\langle \chi_{\mathbf{R}'m'}^{\perp,A} | H^{LDA} - \varepsilon_F | \chi_{\mathbf{R}m}^{\perp,B} \rangle \equiv t_{m',m}^{A-B,\mathbf{R}'-\mathbf{R}}, \quad (1)$$

in a Wannier representation, where the NMTO Wannier

functions $|\chi_{\mathbf{R}m}^{1,A}\rangle$ are orthonormal. Here, $t_{m',m}^{A-B,\mathbf{R}'-\mathbf{R}}$ denotes the hopping term from orbital m of atom B on site \mathbf{R} to the orbital m' of atom A on site \mathbf{R}' (A and B are either Ni or Mn) Further information concerning technical details of the calculation can be found in Ref. 5,27.

In a previous paper²⁷ we discussed the chemical bonding and computed model Hamiltonian parameters for the semi-heusler NiMnSb using only $Mn-d$ Wannier orbitals. As mentioned above, not only the $Mn-d-Sb-p$, but also $Mn-d-Ni-d$ interactions are required to open a gap in the minority spin channel: the minority occupied bonding states are mainly of $Ni-d$ character, while the unoccupied anti-bonding states are mainly of $Mn-d$ character. Therefore, in the present work we consider an enlarged NMTO-basis consisting of Ni - and $Mn-d$ orbitals which span an energy window of about $\pm 3eV$ around the Fermi energy.

The matrix elements for the on-site energies $\epsilon_m^A \equiv t_{m,m}^{A-A,0}$ are given by (we use the convention in which $m = 1, \dots, 5$ corresponds to the d orbitals $\{xy, yz, zx, 3z^2-1, x^2-y^2\}$ in the order)

$$\epsilon_m^{\text{Mn}} = (-1411, -1411, -1411, -721, -721), \quad (2)$$

$$\epsilon_m^{\text{Ni}} = (-2439, -2439, -2439, -2679, -2679). \quad (3)$$

The nearest-neighbour hopping terms are given by ($\Delta_1 \equiv (-\frac{1}{4}, -\frac{1}{4}, -\frac{1}{4})$)

$$t_{m',m}^{\text{Ni-Mn},\Delta_1} = \begin{pmatrix} -153 & -272 & -272 & -153 & 0 \\ -272 & -153 & -272 & 76 & -132 \\ -272 & -272 & -153 & 76 & 0 \\ 110 & -55 & -55 & 1 & 132 \\ 0 & 95 & -95 & 0 & 1 \end{pmatrix},$$

and the next-nearest-neighbour terms ($\Delta_2 \equiv (\frac{1}{2}, -\frac{1}{2}, 0)$)

$$t_{m',m}^{\text{Mn-Mn},\Delta_2} = \begin{pmatrix} -107 & -14 & 14 & 72 & 0 \\ 14 & 6 & 36 & -12 & 4 \\ -14 & 36 & 6 & 12 & 0 \\ 72 & 12 & -12 & 61 & 4 \\ 0 & -4 & -4 & 0 & -52 \end{pmatrix}, \quad (4)$$

$$t_{m',m}^{\text{Ni-Ni},\Delta_2} = \begin{pmatrix} 142 & -53 & 53 & 129 & 0 \\ 53 & 229 & -71 & 133 & -92 \\ -53 & -71 & 229 & -133 & -92 \\ 129 & -133 & 133 & 40 & 0 \\ 0 & 92 & 92 & 0 & -51 \end{pmatrix}. \quad (5)$$

Here, all hoppings are given in units of meV, and only one representative hopping integral is shown for each class. Other hopping terms can be derived from proper unitary transformation using crystal symmetry (see, e.g., Ref. 28 for details). As one can see, the largest hoppings occur between the Wannier orbitals located on Ni - and Mn atoms. In addition, there are further hopping terms in the Hamiltonian, which we don't show here for simplicity. We have taken into account hoppings up to a

range of $r = 2.0a$. Neglected hoppings are about a factor 30 smaller than the largest nearest-neighbor hopping. The non-interacting part of the effective Hamiltonian for NiMnSb, thus, has the form

$$H_0 = \sum_{\mathbf{R}',\mathbf{R},\sigma} \sum_{\{A,B,m',m\}} t_{m',m}^{A-B,\mathbf{R}'-\mathbf{R}} c_{B\mathbf{R}'m'\sigma}^\dagger c_{A\mathbf{R}m\sigma}. \quad (6)$$

To take into account correlation effects, we add the spin-rotation invariant interaction H_I

$$H_I = \frac{1}{2} \sum_{\mathbf{R},A,\sigma} \sum_{m,n,o,p} U_{mnop} c_{A\mathbf{R}m\sigma}^\dagger c_{A\mathbf{R}n\sigma}^\dagger c_{A\mathbf{R}p\sigma} c_{A\mathbf{R}o\sigma} \quad (7)$$

In Eqs. (6) and (7), $c_{A\mathbf{R}m\sigma}$ ($c_{A\mathbf{R}m\sigma}^\dagger$) are the usual fermionic annihilation (creation) operators acting on an electron with spin σ at site \mathbf{R} in the orbital m of atom A . The Hamiltonian we are using includes spin- and pair-flip terms, as especially spin flip processes are important for a correct description of non-quasiparticle states^{5,14}. For a realistic description of Coulomb interactions, the matrix elements U_{mnop} can be computed for the particular material in terms of effective Slater integrals and Racah or Kanamori coefficients^{29,30}. We used for both Mn and Ni the following effective Slater parameters: $F_{\text{Mn/Ni}}^0 = 1.26\text{eV}$, $F_{\text{Mn/Ni}}^2 = 5.58\text{eV}$ and $F_{\text{Mn/Ni}}^4 = 3.49\text{eV}$, which correspond to $U = U_{mmmm} = 2.0\text{eV}$ and give an average $\bar{J} = 0.65\text{eV}$. In addition, we checked that our results do not depend significantly on the chosen U and \bar{J} -values by performing additional calculations for $U = 2.5\text{eV}$ and $U = 3\text{eV}$ with $\bar{J} = 0.77\text{eV}$. The range of values corresponds to the one used in previous works^{12,13,31,32}.

The on-site energies calculated in NMTO already contain effects from the Coulomb interaction at the LDA mean-field level. While this double counting can be absorbed into the chemical potential when only one set of degenerate orbitals is taken into account (see e.g. Refs. 14,33) this is generally not possible if the full d -orbitals and/or the orbitals of more than one inequivalent atom are used as basis set. Consequently, in order to avoid a double counting of the Coulomb contribution, the corresponding Hartree terms have to be subtracted from H_0 .³⁴ This is achieved by replacing the onsite energies ϵ_m^A obtained from NMTO with³⁵

$$\epsilon_m^{\prime A} = \epsilon_m^A - \frac{1}{2} \left\{ U_{mmmm} \langle n_m^A \rangle - \sum_{m' \neq m} (2U_{mm'mm'} - U_{mm'm'm}) \langle n_{m'}^A \rangle \right\}. \quad (8)$$

$\langle n_m^A \rangle$ denotes the occupation of the *NMTO band* associated with atom A and orbital m . Notice that this is different from the occupation of the *orbital* m in atom A . The present double-counting procedure corresponds to the ‘‘around-mean-field’’ scheme^{34,36}. In order to test the dependence on the double-counting schemes, we performed calculations considering different schemes, such as

the “fully-localized” scheme and a combination of these two schemes as discussed in Ref. 34. From these tests, we find that our LDA+VCA results for the spectral function remain unchanged for energies within $E_F \pm 1\text{eV}$, while for energies outside this range (from $\pm 1\text{eV}$ to about $\pm 3\text{eV}$) a redistribution of Mn - and Ni - states is obtained.

B. Variational Cluster Approach

To solve the many-body Hamiltonian (6)+(7), we employ the Variational Cluster Approach^{37,38}. This method is an extension of Cluster Perturbation Theory (CPT)^{39,40,41}. In CPT, the original lattice is divided into a set of disconnected clusters, and the inter-cluster hopping terms are treated perturbatively. VCA additionally includes “virtual” single-particle terms to the cluster Hamiltonian, yielding a so-called reference system, and then subtracts these terms perturbatively. The “optimal” value for these variational parameters is determined in the framework of the Self-energy Functional Approach (SFA)^{42,43}, by requiring that the SFA grand-canonical potential Ω be stationary within this set of variational parameters. In this work, we only include the chemical potential of the cluster as a variational parameter, which is necessary in order to obtain a thermodynamically consistent particle density^{44,45}. It is not necessary to include a ferromagnetic field in order to obtain a ferromagnetic phase, since the symmetry can be broken already at the finite-cluster level³⁵. In this paper, we use a new method, described in Ref. 46, to carry out the sum over Matsubara frequencies required in the evaluation of Ω , whereby an integral over a contour lying a finite (not small) distance from the real axis is carried out.

As a reference system we use a cluster of two sites, representing one Mn -atom and one Ni -atom (see Fig. 1), each having the full- d manifold of five orbitals. Since we have to consider all five orbitals for each atom, it is very difficult to use larger clusters, which have to be exactly diagonalized many times in combination with the variational procedure.

III. RESULTS

A. Density of states

In order to study the influence of correlations on the half-metallic gap, we first display the spin-resolved local density of states in Fig. 2. Here, we present a comparison of the results obtained from LSDA with the results from our LDA+VCA calculation. The LSDA-DOS is mainly characterized by a large exchange splitting (about 3eV) of the Mn - d states, leading to large spin moments on the Mn -site ($3.72\mu_B$). A small induced ferromagnetic moment is present on Ni ($0.29\mu_B$), while the Sb moment ($0.06\mu_B$) is anti-parallel to the Mn moment. Overall, the

calculated moments are in very good agreement with previous ab-initio results^{1,5,23,25,27}. The existence of large localized Mn moments of about $3.78\mu_B$ has been verified experimentally by neutron diffraction⁴⁷ as well as by the sum rule of the x-ray magnetic circular dichroism spectra⁴⁸. These two experiments also confirm the magnitude of the LSDA-computed moments for Ni and Sb . The gap in the minority spin channel is about 0.5eV wide and the total magnetic moment has an integer value of $4\mu_B$. Note, that in Fig. 2 in LSDA the minority occupied bonding states are mainly of Ni - d character, while unoccupied anti-bonding states are mainly of Mn - d character. It was pointed out¹ that the opening of a gap is assisted by Sb through the symmetry lowering with the consequence that the distinction between Mn - t_{2g} and Sb - p character of the electrons is lost.

Concerning the LDA+VCA results, we find a total magnetic moment of $3.7\mu_B$, which is in reasonable agreement with experimental values^{47,48}. In direct comparison

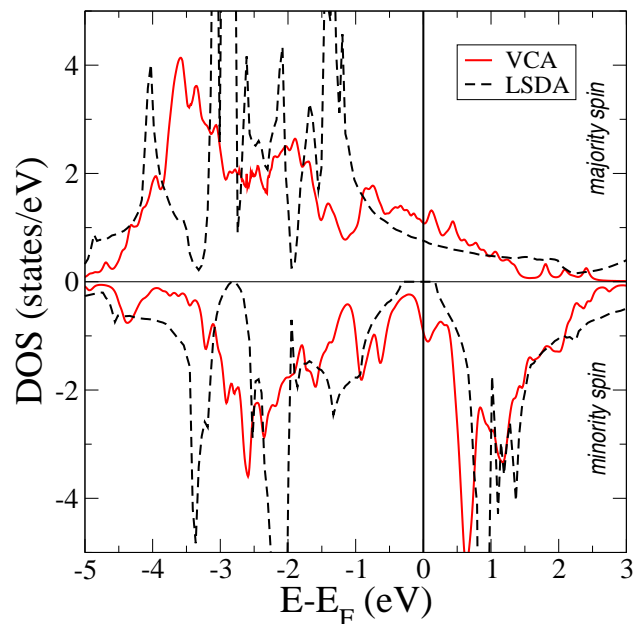


FIG. 2: (Color online) Density of states for NiMnSb obtained from LDA+VCA (red, solid line) for values of the average Coulomb and exchange parameters $U = 2\text{eV}$ and $\bar{J} = 0.65\text{eV}$ for both Mn and Ni atoms. in comparison to results obtained from LSDA (black, dashed line).

to LSDA, our results show that correlation effects do not affect too strongly the general picture of the minority spin DOS for energies which are more than 0.5 eV away from the Fermi energy. In the range $0.5\text{eV} \lesssim E - E_F \lesssim 3\text{eV}$, unoccupied Mn - states are visible in the minority spin sector, similarly to LSDA. However, these states are shifted to lower energies due to a slight reduction of the Mn - exchange splitting generated by the many-body correlations. Just above the Fermi level, NQP states are present, with a peak around the energy of 0.06eV. It is important to note that these states were also obtained in

previous calculations using a LDA+DMFT many-body approach¹² at finite temperatures. In comparison to the DMFT description, the non-local correlations captured by VCA enhance the spectral weight of the NQP states and slightly shift their position. This fact leads to the conclusion that even a local DMFT description is sufficient to demonstrate the existence of NQP states as discussed previously¹². The spectral weight of the NQP states is large enough, so that we expect them to be well pronounced in corresponding experimental data. While model calculations for single-band Hamiltonians⁵ suggest that NQP states should only touch the Fermi level with zero weight at $T = 0K$, in our VCA calculation they maintain a finite weight at the Fermi level, thus leading to a reduction of spin polarisation, even at $T = 0K$. In the LSDA-results, the bonding states below the Fermi level have dominant $Ni-d$ character and are responsible for the gap formation. While these states form a single peak at $-1.5eV$ in LSDA, the LDA+VCA-results show a splitting into two peaks centered around $-1eV$. One of these peaks is pushed closer to the Fermi level, while the other one is shifted to higher energies. The latter correlation effect is also seen in previous LSDA+DMFT results¹².

A significantly stronger effect caused by many-body correlations is visible in the majority-spin channel (see Fig. 2). Here we discuss the behaviour in the same energy range within $\pm 3eV$ around the Fermi level, since this is the energy window spanned by our NMTO basis. The LSDA density of states in this energy range is determined mainly by the covalent $Ni-Mn-d$ hybridization, and by the large exchange splitting of $Mn-d$ electrons^{1,5,27}. At the Fermi level and above a reduced density of states is present. The density of states obtained from the LDA+VCA calculation shows a very strong spectral redistribution for the majority spin electrons: the LSDA peak situated around $-3eV$ is lowered in energy while in the energy range between $-2eV$ and E_F , a spectral-weight transfer towards the Fermi level takes place. In particular, the large LSDA-peak at $-1.5eV$ is shifted to about $-1eV$, which results in a significant contribution to the states at the Fermi level. Just above the Fermi level, at energies where NQP states are formed in the minority-spin channel, a resonance peak is present for the majority-spin electrons. A further maximum of the density of states is present at $0.5eV$. The meaning of this maximum will become clear in the Sec. III B where the \mathbf{k} -resolved spectral functions are discussed. In contrast to our VCA calculation, DMFT results¹² do not change significantly the picture for the majority-spin states. Although the LDA+DMFT density of states shows a similar reduction of spectral weight for the peak at $-2eV$, its position remains unchanged. The differences between these two results might be explained by the fact that within DMFT Mn and Ni atoms are only coupled via the general many-body and charge-self consistency conditions, while correlations are treated independently in the two atoms. In contrast, the present VCA approach exactly

includes correlations on the length scale of the cluster. These interatom correlations are possibly responsible for the splitting of the covalent $Ni-Mn-d$ electron hybridization in the majority spin states. Due to the breaking of this hybridization, the $Mn-d$ exchange splitting is decreased, which could explain the slight shifts of the minority unoccupied and occupied majority $Mn-d$ states.

B. Spectral properties

In order to gain insight into the nonlocal features of the density of states, we compute the \mathbf{k} -resolved spectral function $A(\mathbf{k}, \omega)$. Majority- and minority-spin spectral functions are presented in Figs. 3 and 4, respectively, with \mathbf{k} following high-symmetry points in the Brillouin zone (BZ). The explanation of the main features of the LSDA band structure was provided by *de Groot et. al.* in his pioneering paper¹. Emphasis was placed on the interaction between Mn and Sb connected by the symmetry constraint, while less attention was given to the Ni atom, although Mn and Ni are first-neighbors and a strong hybridization between them is evidenced in the density of states. In our LDA+VCA calculation, $Ni-d$ and $Mn-d$ states are included explicitly, while Sb -states are admixed by the downfolding procedure.

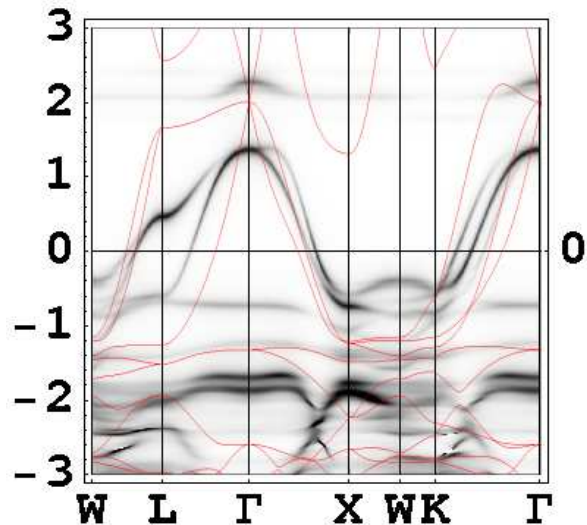


FIG. 3: (Color online) Majority spin LDA+VCA spectral function of NiMnSb (black/white density plot) along the conventional path in the BZ. $W(0.5, 1, 0)$, to $L(0.5, 0.5, 0.5)$ through $\Gamma(0, 0, 0)$, $X(0, 1, 0)$, $K(0, 0.75, 0.75)$ points and ending at $\Gamma(0, 0, 0)$. The LSDA bands (red, thin solid lines) are shown for comparison. Parameters are as in Fig. 2.

Due to correlation, the majority-spin bands crossing the Fermi energy are substantially narrowed with respect to the uncorrelated LSDA bands. Specifically, our results show for the bands crossing the Fermi level a re-

duction of the bandwidth from 3.2eV to 2.2eV. Along the path $W \rightarrow L$ both LSDA bands and the VCA spectral function cross the Fermi level at almost the same k -point. The degenerate unoccupied level situated in the L -symmetry point, around 1.5eV, is strongly pushed towards the Fermi energy, and determines the appearance of the peak visible at 0.5eV in the DOS discussed in Sec. III A. At the same time, correlation effects further split the degenerate levels at the Γ -point seen in LSDA at around 2eV. Note that along $\Gamma \rightarrow X$ crossing of the Fermi level occurs close to the corresponding crossings of the LSDA-bands. Furthermore, along the path $X \rightarrow W \rightarrow K$ both VCA and LSDA bands are only weakly dispersive. However, the VCA bands are shifted towards the Fermi level, while along the line back into the Γ -point, the Fermi-energy crossing of the VCA bands takes place closer to the K -point.

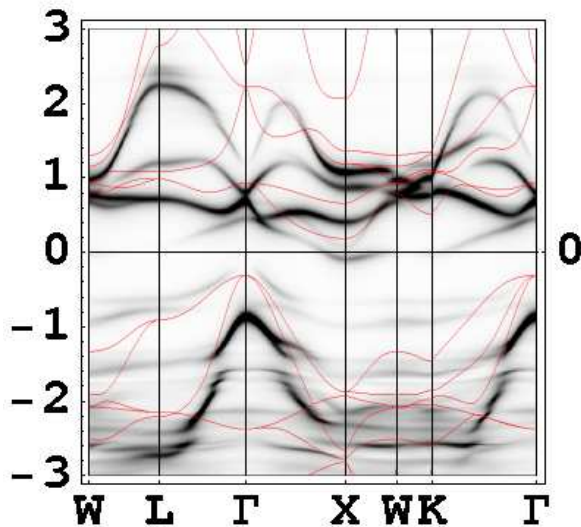


FIG. 4: (Color online) Minority-spin LDA+VCA spectral function of NiMnSb (black/white density plot) along the same BZ path as in Fig. 3. The LSDA bands (red, thin solid lines) are shown for comparison. Parameters are as in Fig. 2.

The minority-spin band structure of LSDA shows an indirect gap of about 0.5eV between Γ and X -point. Within this indirect gap formed by the mostly $Ni-d$ occupied and mostly $Mn-d$ unoccupied states, the LDA+VCA results show substantial spectral weight, as can be seen in Fig. 4. Notably, across the Fermi level a weakly-dispersive band is present, centered around 0.1eV, representing the NQP states. At higher energies, in the range of 1 to 2eV above E_F , the VCA bands are substantially correlation-narrowed with respect to LSDA. The features above the Fermi level, including the non-quasiparticle states, have dominant $Mn-d$ character. Below the Fermi level, correlations split off the occupied bands having mainly $Ni-d$ character. The spectral weight is redistributed: a part is transferred towards the Fermi

level, however with smaller weight, while most weight is transferred towards higher binding energies. The same effect is visible in the density of states plot displayed in Fig. 2. Notice that while the shift towards higher binding energies is also seen in the previous LSDA+DMFT calculation¹², the weak shift towards the Fermi level is only obtained within the present calculation.

In order to explore correlation effects in more detail, we plot in Fig. 5 the self-energy on Mn sites. in the energy range ± 2 eV around the Fermi level and near the Fermi crossing at $k = (0.5, 0.7, 0.3)\pi/a$. The upper/lower panel of Fig. 5 shows the spin resolved real/imaginary part of the electronic Mn self-energy.

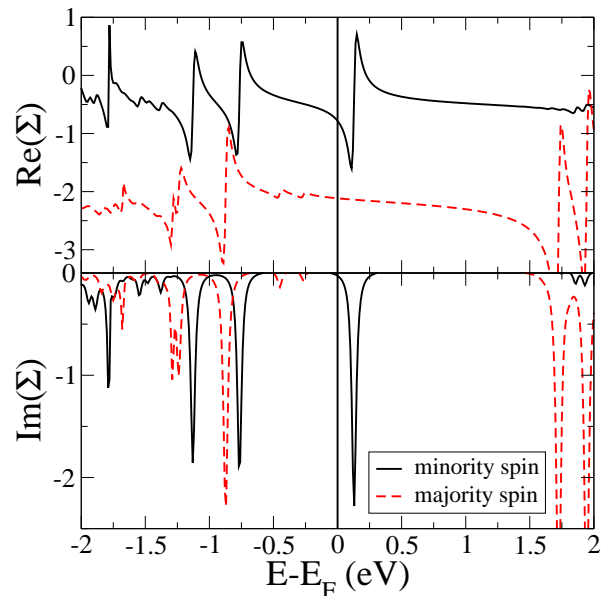


FIG. 5: (color online) Spin resolved self-energy on $Mn-d$ orbitals, at the crossing point $k = (0.5, 0.7, 0.3)$.

Below E_F , the minority-spin self-energy is similar to the self-energy of the majority spin channel. Just above the Fermi level, however, a clear peak in $\text{Im}(\Sigma_{VCA}^\downarrow)$ is present with a maximum around the energies of the non-quasiparticle states (Fig. 2 and Fig. 4). In previous DMFT calculations¹², a very similar behaviour of the imaginary part of the local self-energy was seen. In that case, the pronounced feature above E_F was attributed to the minority $Mn-d(t_{2g})$ states. The real part of the self-energy displays a negative slope $\partial\Sigma/\partial\omega < 0$ at the Fermi energy for both spin directions, which confirms that the quasiparticle weight $Z = (1 - \frac{\partial\Sigma}{\partial\omega})^{-1}$ is reduced by correlations. However, while for majority spins $|\partial\Sigma_\uparrow/\partial\omega|$ is clearly less than unity, for minority spins $|\partial\Sigma_\downarrow/\partial\omega| \gtrsim 1$ (within our approximation, we cannot determine Σ with sufficient accuracy), suggesting the nonquasiparticle nature of the minority spin states within the gap.

C. Low-energy spin polarization and comparison with experiments

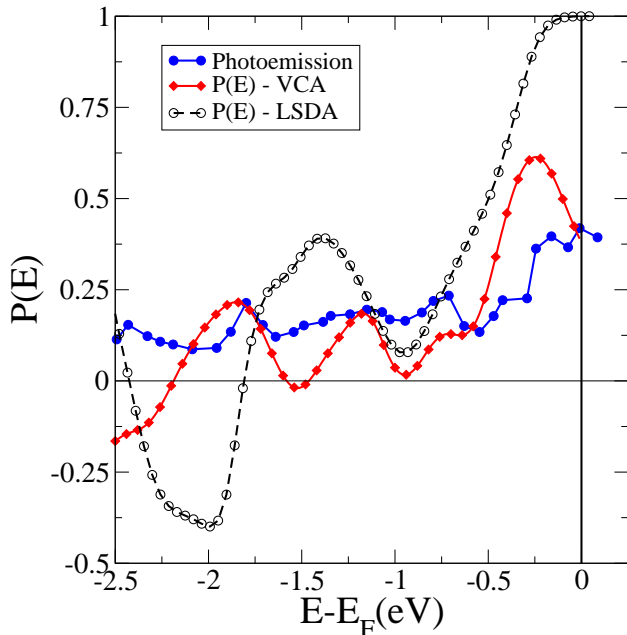


FIG. 6: (Color online) Energy-dependent polarization obtained from LSDA and LDA+VCA in comparison with data from spin-polarized photoemission⁸.

To investigate the consequences of the modification of majority and minority spectral weight at the Fermi energy produced by correlations, we turn to the issue of the spin polarization. This is given by the expression $P(E) = (N_{\uparrow}(E) - N_{\downarrow}(E)) / (N_{\uparrow}(E) + N_{\downarrow}(E))$, $N_{\sigma}(E)$ being the spin-resolved density of states, and is plotted in Fig. 6 as a function of energy measured from the Fermi level. The computed LSDA and VCA values are compared with the raw data obtained from spin-resolved photoemission measurement by Zhou et al.⁸ For this comparison, the density of states was multiplied with the Fermi function and a Gaussian broadening of 100meV was used to account for experimental resolution. *Zhu et al.*⁸ discuss the appearance of a shoulder close to the Fermi level when proper annealing is performed to restore the stoichiometry in NiMnSb. This shoulder is visible in the majority spin channel (Fig.2c from Ref. 8) and could be an indication for the correlation-induced spectral weight transfer of the majority spin states, not present in the LSDA calculations. In addition, the value

of the spin polarization at the Fermi level obtained from our LDA+VCA-results is situated in the interval of values reported experimentally^{2,8,49}.

IV. SUMMARY

We have investigated the effects of correlations in NiMnSb using a combined LDA+VCA approach. The parameters for the effective non-interacting Hamiltonian were obtained using the downfolding procedure, for a basis including *Ni* and *Mn-d* orbitals. The multi-orbital Hubbard-type many-body Hamiltonian was solved using the Variational Cluster Approach for different values of $U_{Mn/Ni}$ in the range of 2 – 3eV and $\bar{J}_{Mn/Ni} = 0.65/0.78$ eV. The results presented do not show significant differences for the studied range of parameters, nor for different double-counting procedures used. We showed that the presence of *Ni-d* orbitals in the NMTO-basis allows for a more complete description of the low-energy behavior of NiMnSb. In particular, it correctly describes the spectral weight transfer towards the Fermi level in the majority spin channel and the formation of minority-spin states with vanishing quasiparticle weight (NQP states) just above the Fermi level. The analysis of the minority-spin spectral function shows for the NQP states a weakly dispersive band having dominantly *Mn-d* character. Due to electron correlations, the covalent *Ni-Mn d*-hybridization in the majority-spin channel splits up and part of the weight is transferred towards the Fermi level. The *simultaneous* presence of majority spin spectral weight transfer towards the Fermi level, and the occurrence of minority-spin non-quasiparticle states emphasizes the importance of correlation effects in this material, despite the small value of U .

Despite the fact that high-quality films of NiMnSb have been grown, they do not reproduce the half-metallic character of the bulk detected by spin-polarized positron-annihilation^{6,7}. On the other hand, one should mention that the positron annihilation technique only provides an evidence for half metallicity by means of a consistency check. In other words, the “proof” is carried out by modeling the data assuming a half-metallic band structure, with a full minority spin gap, *from the outset*^{6,7}. For this reason, it would be interesting to revisit the analysis of the positron-annihilation data by using the correlated band structure obtained here, i. e., by taking into account the existence of NQP states.

We acknowledge financial support by the Austrian science fund (FWF project P18505-N16), and by the cooperation project “NAWI Graz” (F-NW-515-GASS).

* hannes.allmaier@itp.tugraz.at

¹ R. A. de Groot, F. M. Mueller, P. G. van Engen, and K. H. J. Buschow, Phys. Rev. Lett. **50**, 2024 (1983).

² R. J. Soulen et al., Science **282**, 85 (1998).

³ I. Zutic, J. Fabian, and S. D. Sarma, Rev. Mod. Phys. **76**,

323 (2004).

⁴ G. A. de Wijs and R. A. de Groot, Phys. Rev. B **64**, 020402 (2001).

⁵ M. I. Katsnelson et al., Reviews of Modern Physics **80**, 315 (2008).

- ⁶ K. E. H. M. Hanssen and P. E. Mijnders, Phys. Rev. B **34**, 5009 (1986).
- ⁷ K. E. H. M. Hanssen, P. E. Mijnders, L. P. L. M. Rabou, and K. H. J. Buschow, Phys. Rev. B **42**, 1533 (1990).
- ⁸ W. Zhu *et al.*, Phys. Rev. B **64**, 060403 (2001).
- ⁹ J. S. Correa *et al.*, Phys. Rev. B **73**, 125316 (2006).
- ¹⁰ J. Minar, J. Braun, S. Bornemann, and M. Donath, J. Phys. D: Appl. Phys. **42**, 084009 (1999).
- ¹¹ J. Liu *et al.*, J. Appl. Phys. **99**, 036110 (2006).
- ¹² L. Chioncel, M. I. Katsnelson, R. A. de Groot, and A. I. Lichtenstein, Phys. Rev. B **68**, 144425 (2003).
- ¹³ L. Chioncel *et al.*, Phys. Rev. Lett. **96**, 197203 (2006).
- ¹⁴ L. Chioncel *et al.*, Phys. Rev. B **75**, 140406 (2007).
- ¹⁵ L. Chioncel *et al.*, Phys. Rev. Lett. **100**, 086402 (2008).
- ¹⁶ L. Chioncel, E. Arrigoni, M. I. Katsnelson, and A. I. Lichtenstein, Phys. Rev. B **79**, 125123 (2009).
- ¹⁷ D. M. Edwards and J. A. Hertz, Journal of Physics F-Metal Physics **3**, 2191 (1973).
- ¹⁸ V. Y. Irkhin and M. I. Katsnelson, J. Phys.: Condens. Matter **2**, 7151 (1990).
- ¹⁹ H. Allmaier *et al.*, J. Optoelectronics Adv. Mat. **10**, 1671 (2008).
- ²⁰ O. K. Andersen and T. Saha-Dasgupta, Phys. Rev. B **62**, R16219 (2000).
- ²¹ E. Zurek, O. Jepsen, and O. K. Andersen, ChemPhysChem **6**, 1934 (2005).
- ²² S. Ögüt and K. M. Rabe, Phys. Rev. B **51**, 10443 (1995).
- ²³ I. Galanakis, P. H. Dederichs, and N. Papanikolaou, Phys. Rev. B **66**, 134428 (2002).
- ²⁴ B. R. K. Nanda and I. Dasgupta, J. Phys.: Condens. Matter **15**, 7307 (2003).
- ²⁵ E. Kulatov and I. I. Mazin, J. Phys.: Condens. Matter **2**, 343 (1990).
- ²⁶ O. K. Andersen and O. Jepsen, Phys. Rev. Lett. **53**, 2571 (1984).
- ²⁷ A. Yamasaki, L. Chioncel, A. I. Lichtenstein, and O. K. Andersen, Phys. Rev. B **74**, 024419 (2006).
- ²⁸ E. Pavarini, A. Yamasaki, J. Nuss, and O. K. Andersen, New J. Phys. **7**, 188 (2005).
- ²⁹ M. Imada, A. Fujimori, and Y. Tokura, Rev. Mod. Phys. **70**, 1039 (1998).
- ³⁰ G. Kotliar *et al.*, Rev. Mod. Phys. **78**, 865 (2006).
- ³¹ L. Chioncel *et al.*, Phys. Rev. B **71**, 085111 (2005).
- ³² L. Chioncel, E. Arrigoni, M. I. Katsnelson, and A. I. Lichtenstein, Phys. Rev. Lett. **96**, 137203 (2006).
- ³³ H. Allmaier, L. Chioncel, and E. Arrigoni, Phys. Rev. B **79**, 235126 (2009).
- ³⁴ A. G. Petukhov, I. I. Mazin, L. Chioncel, and A. I. Lichtenstein, Phys. Rev. B **67**, 153106 (2003).
- ³⁵ Notice that the initial NMTO calculation is carried out in the nonmagnetic phase, so that the starting Hamiltonian (6) plus (7) is spin independent. The ferromagnetic solution is then obtained variationally within the VCA approach. This is important in order to preserve a spin-rotation symmetric model Hamiltonian.
- ³⁶ M. T. Czyzyk and G. A. Sawatzky, Phys. Rev. B **49**, 14211 (1994).
- ³⁷ M. Potthoff, M. Aichhorn, and C. Dahnken, Phys. Rev. Lett. **91**, 206402 (2003).
- ³⁸ C. Dahnken *et al.*, Phys. Rev. B **70**, 245110 (2004).
- ³⁹ C. Gros and R. Valenti, Phys. Rev. B **48**, 418 (1993).
- ⁴⁰ D. Sénéchal, D. Perez, and M. Pioro-Ladriere, Phys. Rev. Lett. **84**, 522 (2000).
- ⁴¹ S. G. Ovchinnikov and I. S. Sandalov, Physica C **161**, 607 (1989).
- ⁴² M. Potthoff, Eur. Phys. J. B **32**, 429 (2003).
- ⁴³ M. Potthoff, Eur. Phys. J. B **36**, 335 (2003).
- ⁴⁴ M. Aichhorn and E. Arrigoni, Europhys. Lett. **72**, 117 (2005).
- ⁴⁵ M. Aichhorn, E. Arrigoni, M. Potthoff, and W. Hanke, Phys. Rev. B **74**, 024508 (2006).
- ⁴⁶ X. Lu and E. Arrigoni, Phys. Rev. B **79**, 245109 (2009).
- ⁴⁷ C. Hordequin, J. Pierre, and R. Currat, Physica B **234-236**, 605 (1997).
- ⁴⁸ A. Kimura *et al.*, Phys. Rev. B **56**, 6021 (1997).
- ⁴⁹ S. K. Clowes *et al.*, Phys. Rev. B **69**, 214425 (2004).